ACS OMEGA

http://pubs.acs.org/journal/acsodf

Article

Microporous Structure Formation of Poly(methyl methacrylate) via Polymerization-Induced Phase Separation in the Presence of Poly(ethylene glycol)

Yasuhito Suzuki,* Shodai Onozato, Yuya Shinagawa, and Akikazu Matsumoto

Cite This: *ACS Omega* 2022, 7, 38933−38941

Read Online

ACCESS | Metrics & More | Article Recommendations | Supporting Information

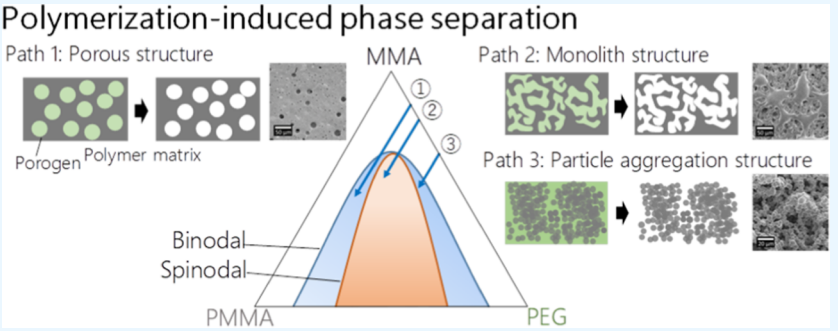

ABSTRACT: It has been demonstrated that nano- or micro-structured polymeric materials have huge potential as advanced materials. However, most of the current fabricating methods have limitations either in cost or in size. Here, we investigate the bulk polymerization of methyl methacrylate in the presence of poly(ethylene glycol) (PEG). We found that phase separation occurs during bulk polymerization. After removal of PEG via sonication, microscopic structures of poly(methyl methacrylate), including porous structures, co-continuous monolith structures, or particle aggregation structures, are formed. These structures can be controlled by the amount of PEG added and the reaction temperature. The results are summarized in phase diagrams. The addition of PEG significantly affects the reaction kinetics. Phase separation is coupled with the reaction acceleration known as the Trommsdorff effect. As a result, the reaction completes in a shorter time when the PEG amount is higher. We demonstrate surface coating to fabricate an amphiphobic surface, repelling both water and oil. The methods presented here have the potential to fabricate microscopic structures in large areas cost-effectively.

INTRODUCTION

Microscopically structured materials have been fabricated, and their distinct properties have been demonstrated.[1,2] Their application spans cell adhesion surfaces,[3] microreactors,[4] and photonics.[5] They can also be used to control wettability.[6−8] However, in many cases, sophisticated methods have been applied on a small scale.[1,9−11] For practical applications, it is necessary to fabricate such structures in cost-effective ways on a large scale. Poly(methyl methacrylate) (PMMA) is a widely used polymer for applications including acrylic windows,[12] coatings,[13] and adhesives.[14] Due to the UV resistance of PMMA,[15] it can also be used outside. Additionally, PMMA can be a sustainable material through recycling via monomer recovery.[16] Therefore, microstructured PMMA has potential as a high-performance material. It was reported that while the mixture of ethanol and PMMA is miscible at 60 °C, phase separation occurs upon cooling and forms a co-continuous monolith.[17] Another approach is the use of polymerization-induced phase separation. MMA was polymerized in the presence of polystyrene (PSt).[18] While PSt is soluble in MMA, PSt and PMMA tend to phase separate. The third component, whose purpose is to generate phase separation, is called porogen. Depending on the temperature and combination of porogens, different structures are formed. Recently, it was reported that the bulk polymerization of MMA in a swelled PSt matrix leads to structured PMMA particles in the matrix, leading to a blue structural color.[19] Microstructure formation using phase separation has been investigated in a variety of materials. For example, the curing of the epoxy resin in the presence of poly(ethylene glycol) (PEG) leads to a co-continuous monolith structure.[20,21] The epoxy monolith has been applied for separation technologies,[22,23] multi-material

Received: July 25, 2022
Accepted: October 12, 2022
Published: October 21, 2022

https://doi.org/10.1021/acsomega.2c04690
ACS Omega 2022, 7, 38933−38941

bonding,[24−26] and novel tough co-continuous network materials.[27]

During bulk polymerization of MMA, a sudden temperature increase known as the Trommsdorff effect may occur.[28−30] Classically, it has long been attributed to the increased viscosity and decreased termination rate. The critical factor is the apparent termination rate coefficient, which depends on the chain length and monomer conversion.[31,32] However, the detailed mechanism of the Trommsdorff effect is complex and still elusive.[30] The cage effect and the glass effect may also be operative.[33] Recent research suggests that the Trommsdorff effect is intimately related to the heterogeneity that arises at some point during bulk polymerization.[34−37] Our previous research studies report that the polymerization-induced phase separation of MMA occurs at the same time as the Trommsdorff effect.[38]

In this study, we investigated the structure formation of PMMA when it was prepared via bulk polymerization in the presence of PEG. Although PEG behaves as a solvent in some sense, we use the terminology bulk polymerization in this study because the solid glassy polymer is directly obtained in this process. Previous research reported that the polymerization kinetics of MMA is significantly accelerated in PEG in comparison to the kinetics in toluene.[39] They also pointed out that the so-called microviscosity of MMA, which is a local viscosity that governs the reaction kinetics, may differ in the presence of PEG. Therefore, we are interested in the effect of addition of PEG on the bulk polymerization of MMA. In this study, we focus only on free radical polymerization. We show that porous structures, co-continuous monolith structures, or particle aggregation structures are formed depending on the initial conditions. We discuss the onset of phase separation and construct phase diagrams. Lastly, it is demonstrated that fluorinated particle aggregation structures have amphiphobicity, repelling both water and oil. This approach provides the possibility to fabricate microstructured surfaces for advanced properties in large areas inexpensively.

EXPERIMENTAL METHODS

Materials. MMA and PEG with different average molar masses were obtained from a commercial source (NACALAI TESQUE, Kyoto, Japan). Prior to use, the inhibitor was removed from MMA with inhibitor removers for removing hydroquinone and monomethyl ether hydroquinone, purchased from Sigma-Aldrich. 2,2′-Azobis(4-methoxy-2,4-dimethylvaleronitrile) (V-70) was purchased from Fujifilm Wako Pure Chemical Corporation, Tokyo, Japan, and used without further purification.

Sample Fabrication. Polymerization-induced structure formation was performed in 20 mL glass vials. Nitrogen gas was bubbled in MMA for approximately 1 min to reduce the dissolved oxygen. In the vial, MMA, V-70, and PEG are mixed. The vial was placed in an oil bath kept at a constant temperature. The reaction mixtures were not stirred upon polymerization. After the chemical reaction, the vial was broken with a hammer. The obtained polymer was immersed in distilled water and sonicated to remove the PEG. The polymer was dried under vacuum for 3 h at 50 °C. The temperature profile was monitored using a k-type thermocouple. The thermocouple was fixed outside of the glass container using Kapton tape. The fabrication temperature was either at room temperature (i.e., 23−25 °C), 30, 35, or 40 °C. The PEG contents range from 10 to 70 wt % with respect to the amount of MMA. The initiator concentration is in the range of 0.1 to 0.6 mol % with respect to the amount of MMA, except for the data presented in Figure 1.

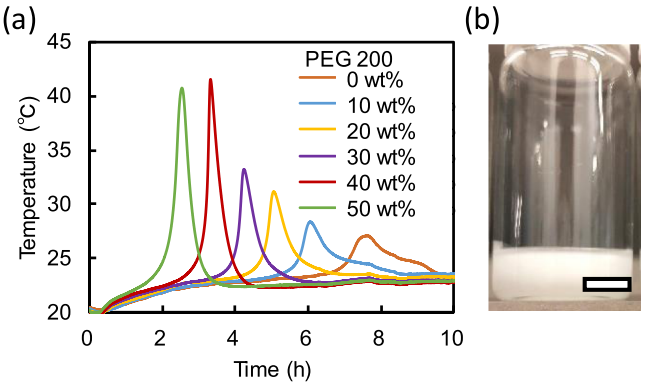

Figure 1. (a) Temperature profile as a function of reaction time during bulk polymerization of MMA in the presence of PEG 200 at room temperature. The PEG content is from 0 to 50 wt %. The initiator concentration was 1.8 mol % with respect to the monomer. (b) When the PEG content is higher than 20 wt %, the final product is opaque. This indicates the formation of a microscopic structure which scatters light. The scale bar is 1 cm.

Scanning Electron Microscopy. Scanning electron microscopy (SEM) using VE-9800 (Keyence Corporation, Ltd., Osaka, Japan) was applied to characterize the surface structure image using an acceleration voltage of 1.0 kV. While we focus on the surface structure in this study, we also checked the structure of the cross-section. In order to obtain cross-sectional images, the sample was immersed in liquid nitrogen and subsequently broken using a hammer. A photograph of the broken sample is provided in Figure S2. SEM images are taken from the top of the structured PMMA as it is. Some cross-sectional images are provided in Figures S3 and S4. Based on SEM images, particle sizes were analyzed using ImageJ, which is open-source software for processing and analyzing scientific images.

Nuclear Magnetic Resonance Spectroscopy. ^{1}H nuclear magnetic resonance (NMR) measurements were conducted to check the conversion. At each reaction time, the vial was placed in liquid nitrogen in order to freeze the sample. Subsequently, the sample was dissolved in deuterated chloroform. ^{1}H NMR spectra were obtained using JEOL ECX-400. The conversion was estimated by the integral ratio from peaks originating from a monomer and a polymer. An example of the ^{1}H NMR spectra with assignment is provided in Figure S1.

Transmittance Measurement. The transmittance at a wave length of 400 nm was recorded during the polymerization. A UV-2600 (Shimadzu Corporation, Kyoto, Japan) spectrophotometer was used. The temperature was controlled using a Peltier temperature controller, TCC-100, from the same company. After initiating the polymerization in a larger glass container, the sample was moved to a UV cell.

Contact Angle Measurement. Contact angle measurements were performed using DMs-400 (Kyowa Interface Science Co., Ltd., Saitama, Japan). 2 μL of a water droplet or a 5 μL of hexadecane droplet was placed on the surface via a syringe dispenser. The static, advancing, and receding contact

https://doi.org/10.1021/acsomega.2c04690
ACS Omega 2022, 7, 38933−38941

angles were obtained using the pre-installed analysis software with the instrument provided by the same company.

Size Exclusion Chromatography. Similar to the sample preparation for ^{1}H NMR, at a certain reaction time, the vial was placed in liquid nitrogen. Then, the sample was dissolved in a fixed amount (300 mL) of THF. The molar mass distribution was analyzed by SEC. The Tosoh TSK-gel GMHHR-N was used as a column which was placed in a thermostat chamber (Chromato Science CS-300 C) kept at 40 °C. The RI detector (JASCO RI-2031-Plus) was used. The flow rate was 0.8 mL/min. The molar mass was calibrated with a polystyrene standard from M_n = 2890 to M_n = 965,000 g/mol.

RESULTS AND DISCUSSION

Figure 1a shows the temperature profile during bulk polymerization of MMA in the presence of different amounts of PEG at room temperature. Since the reaction is exothermic, the temperature is always higher than the ambient temperature during the reaction. When no PEG is added, at the initial stage of the reaction for approximately 7 h, the temperature remains almost constant, indicating that the heat generation and heat dissipation via heat transfer is balanced. At about 7 h after initiation, the temperature increases suddenly, reflecting the acceleration in the reaction. This reaction acceleration is known as the Trommsdorff effect. It is classically attributed to the increased viscosity and decreased termination rate. However, the detailed mechanism of the acceleration is still under debate.[31,33,40] Interestingly, the onset of the Trommsdorff effect systematically shortens as the amount of PEG increases. In the presence of 50 wt % PEG, it takes less than 2 h for the onset of the reaction acceleration. After 2.5 h of the initiation, the maximum temperature reaches 41 °C. Here, PEG is a non-reactive component, and the monomer to initiator ratio is fixed. It is noted that PEG with an average molar mass of 200 g/mol is in a liquid state at room temperature, and hence, the increase in viscosity is limited. It is well known that the pre-dissolved PMMA in MMA shortens the onset of the Trommsdorff effect.[41] This effect is explained by the increased viscosity. On the other hand, the data imply that the reaction acceleration occurs without significantly increased viscosity. Previous research investigated the effect of addition of ethylene glycol dimethyl ether and diethylene glycol dimethyl ether on MMA polymerization in toluene.[39] Their molar masses are 90 and 134 g/mol, respectively. They show only a slight acceleration in reaction kinetics with these low molar mass molecules containing the PEG segments. On the other hand, our data depict a significant increase in reaction kinetics with PEG, whose average molar mass is 200 g/mol. It implies that different mechanisms of reaction acceleration in a solvent may enhance the reaction acceleration in bulk polymerization. As it is discussed below, phase separation is intimately related to the reaction acceleration in bulk. When the initial PEG content is higher than 25 wt %, the reaction acceleration starts and the final product is opaque, as shown in Figure 1b. Since both PMMA and PEG oligomers are transparent, it indicates phase separation. Due to the slightly different refractive indices of MMA and PMMA, an inhomogeneous mixture of them scatters visible light. In order to better understand the timing of phase separation, the transmittance is traced during bulk polymerization using light with a wavelength of 400 nm. Figure 2 depicts a transmittance change as a function of reaction time during the reaction with a

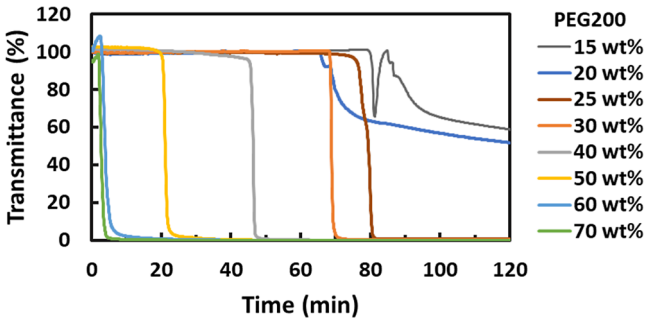

Figure 2. Transmittance as a function of reaction time during bulk polymerization of MMA in the presence of different amounts of PEG ranging from 0 to 70 wt % at 40 °C. The initiator concentration was 0.3 mol % with respect to the monomer.

0.32 mol % initiator at 40 °C. It is noted that while transmittance is suitable for detecting the onset of phase separation, the absolute value of transmittance cannot be discussed in detail. It is strongly affected by bubble or crack formation. They can either increase or decrease the absolute value of transmittance depending on their size and geometry. When PEG content is lower than 20 wt %, the mixture becomes macroscopically inhomogeneous as shown in Figure S5. Therefore, the value of transmittance is not nearly zero. Simultaneous measurements of temperature and transmittance are displayed in Figure 3. As we have recently reported, even in the absence of PEG, a slight decrease in transmittance is observed.[36] After a decrease in transmittance for a while, the value of transmittance recovers. The decrease in transmittance and the increase in temperature occur at the same time. In the same plot in Figure 3, the temperature profile is also displayed. Recent research studies suggest the relationship between the Trommsdorff effect and the apparent phase separation.[36−38] These data support phase separation, which is related to the Trommsdorff effect. The relation between phase separation and Trommsdorff effect is also reported when poly(styrene) is added in photopolymerization of MMA.[37] Therefore, it implies that phase separation plays a crucial role in the Trommsdorff effect. When the PEG content is 40 wt %, it seems that phase separation occurs, possibly faster than the onset of the Trommsdorff effect. Nevertheless, it is difficult to judge the onset of the Trommsdorff effect. The detailed analysis of the relation between phase separation and Trommsdorff effect is beyond the scope of this study. It would require a detailed investigation of the apparent termination rate coefficients in conjunction with the detection of apparent phase separation.

Figure 4 displays SEM images of PMMA polymerized in the presence of PEG with different amounts. As it is described in the experimental section, PEG is washed away after the polymerization via sonication. Therefore, it is mainly the structured PMMA. Depending on the initial amount of PEG, the surface structures are different. Considering the data at 35 °C, when the initial PEG content is 20−30 wt %, porous structures are observed. The pore diameters are in the range from 5 to 100 μm. It is noted that different structures are observed when the PEG content is 30 wt % at different positions of the same sample. These images are also displayed in Figure 4. Above 35 wt % of initial PEG content, bicontinuous monolith structures are formed. The monolith structures always contain aggregated PMMA particles. The amount of aggregated PMMA particles tends to increase as the PEG content increases. The formation mechanism is to be

https://doi.org/10.1021/acsomega.2c04690
ACS Omega 2022, 7, 38933−38941

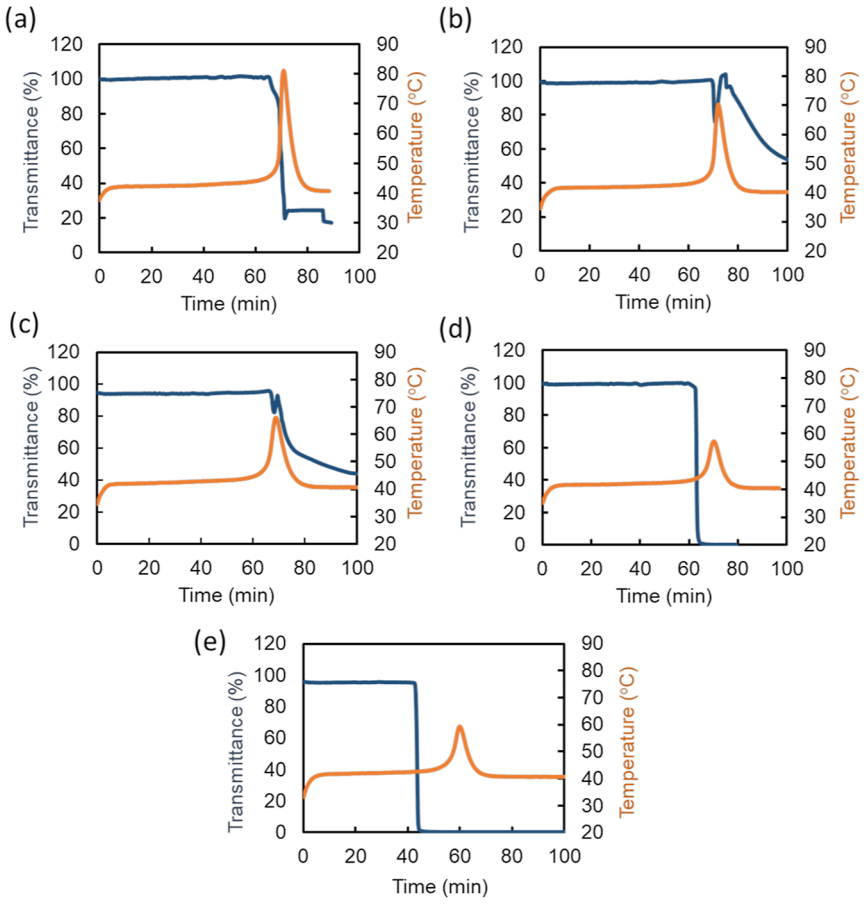

Figure 3. Simultaneous measurements of transmittance and temperature increase during bulk polymerization of MMA in the presence of PEG 200 at 40° C. The PEG 200 contents were (a) 0, (b) 10, (c) 20, (d) 30, and (e) 40%, respectively. The initiator concentration was 0.3 mol % with respect to the monomer.

discussed later in conjunction with the phase diagram. The formed structures are slightly different when prepared at 30 °C, but the general trend is similar. In Figure 5, the effect of initiator concentration on the structure of particle aggregation is shown. The averaged particle sizes are summarized in Table 1. The initiator concentrations varied from 0.1 to 0.6 mol % with respect to the PMMA amount. When the initiator concentration is low, the particle sizes are relatively homogeneous. Especially, the particle sizes are uniform with 0.2 mol % initiator concentrations. The particle sizes are 4.65 ± 0.72 μm in the presence of 40 wt % PEG. On the other hand, with an initiator concentration of 0.6 mol %, multiscale particles are observed. For example, a particle with a 4 μm diameter sticks to a larger particle with a 20 μm diameter. There is a trend that the particle size becomes larger and inhomogeneous as the initiator concentration increases.

Figure 6 shows a model phase diagram of three components, including the monomer, polymer, and porogen.[42] This type of phase diagram can be derived from a classical theory developed by Flory and Huggins.[43,44] This theory is based on thermodynamics. The Flory−Huggins interaction parameter determines the phase state. In this phase diagram, it is assumed that phase separation occurs between the polymer and the porogen. In between the bimodal line and the spinodal line, phase separation occurs via nucleation and growth mechanism. In the case of PEG as a porogen, it is washed away eventually in the sonication process. Inside the spinodal line, phase separation occurs spontaneously. During the polymerization, the amount of the porogen is fixed while the ratio between monomer and polymer changes continuously. Three different scenarios can be considered, as indicated by the three lines in the diagram. In path 1, phase separation occurs only via nucleation and growth mechanisms. Polymer is the major component. Therefore, porogen particles are formed in the polymer matrix. After the removal of porogen, a porous structure is formed. Path 2 depicts the ideal scenario of spinodal decomposition. The spontaneous spinodal decomposition provides a bicontinuous monolith structure. Lastly, as path 3 indicates, nucleation and growth of polymers occur when the polymer component becomes smaller. In this case, polymer particles are formed in the porogen matrix. Eventually, a particle aggregation structure is obtained when porogen is removed. In reality, polymerization-induced phase separation is more complicated. The structure is not fully fixed, while the reaction continuously changes the polymer/monomer ratio. In addition, phase separation changes the chemical compositions of the new phases. We do not discuss multiple phase separations in the newly created phases.

In Figure 7, the apparent phase diagram of MMA, PMMA, and PEG is summarized. First, phase separation was determined by the decrease in transmittance. In a separate experiment under the same conditions, the reaction was stopped at the time of phase separation by immersing it in liquid nitrogen. The obtained sample was dissolved in deuterated chloroform to measure NMR. Based on NMR data, the fraction of MMA and PMMA at the phase separation

https://doi.org/10.1021/acsomega.2c04690
ACS Omega 2022, 7, 38933−38941

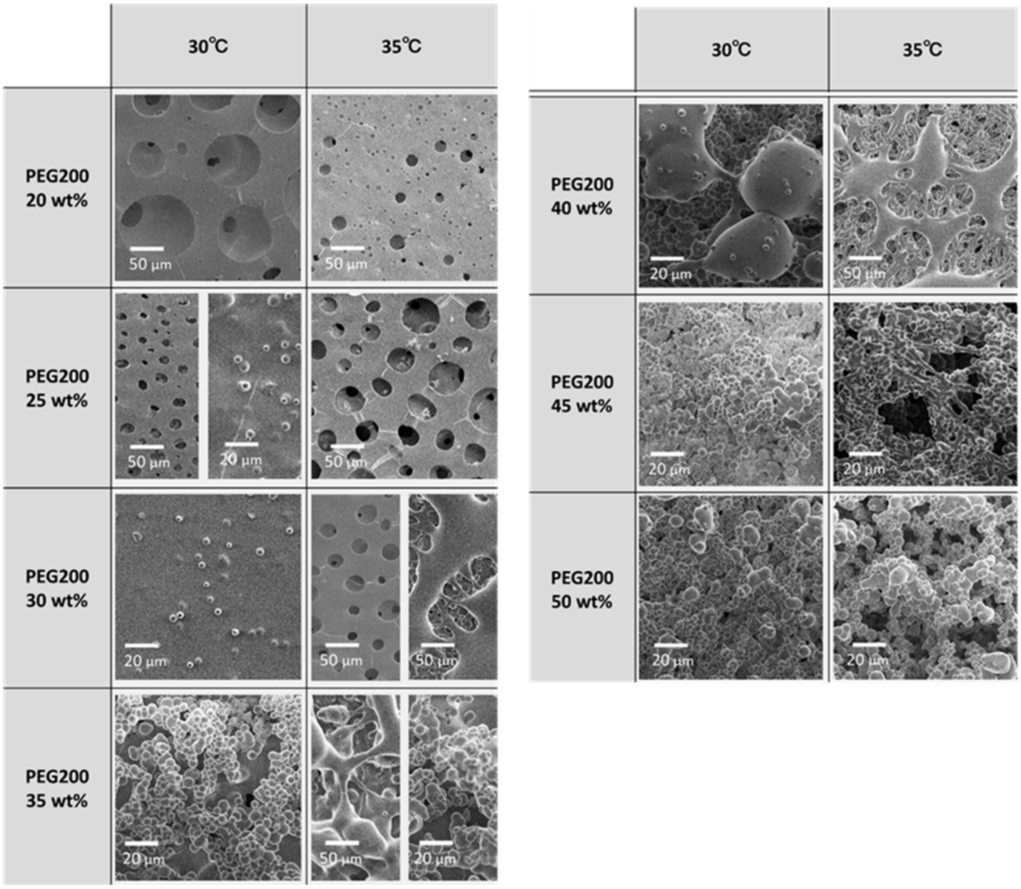

Figure 4. Selected SEM images of the surface structures of PMMA polymerized under different PEG concentrations at 30 or at 35 °C. The SEM images are taken from the top of the obtained PMMA structure without any treatment. In most cases, the structure is similar at different positions. However, in some cases, the structure differs in the middle of the sample and at the rim of the surface. In this case, both images are displayed in the same condition. The initiator concentration was 0.3 mol %.

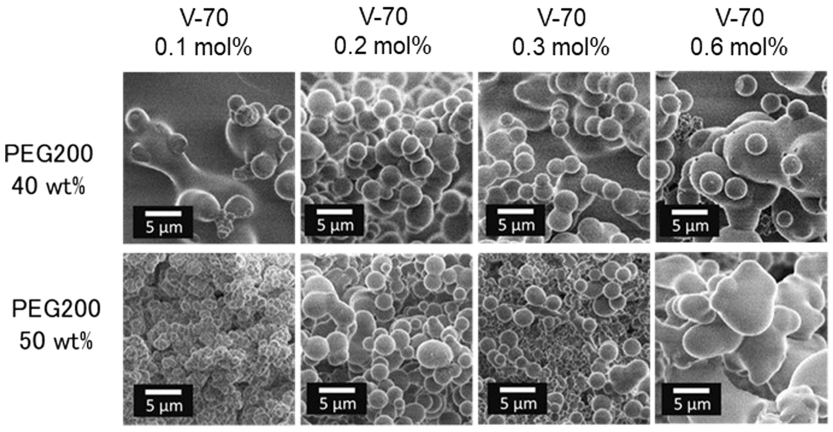

Figure 5. Effect of initiator concentrations on the size and distributions of the particles. The sample was prepared at room temperature.

Table 1. Average Size of the Particles Formed under Different Conditions with the Standard Deviation

	concentration of the initiator (V-70)			
	0.1 mol % (μm)	0.2 mol % (μm)	0.3 mol % (μm)	0.6 mol % (μm)
PEG 200 40 wt %	6.77 ± 2.73	4.65 ± 0.72	5.25 ± 1.24	7.33 ± 3.85
PEG 200 50 wt %	1.95 ± 0.27	4.15 ± 1.07	3.11 ± 0.83	7.86 ± 4.18

was determined. The corresponding SEM images are also shown. It is noted that the SEM images are taken after the completion of the reaction. In addition, PEG segments are washed away. Therefore, it is not precisely the same structure as the point of phase separation. Some experiments are conducted twice under the same condition. They are plotted in

https://doi.org/10.1021/acsomega.2c04690
ACS Omega 2022, 7, 38933−38941

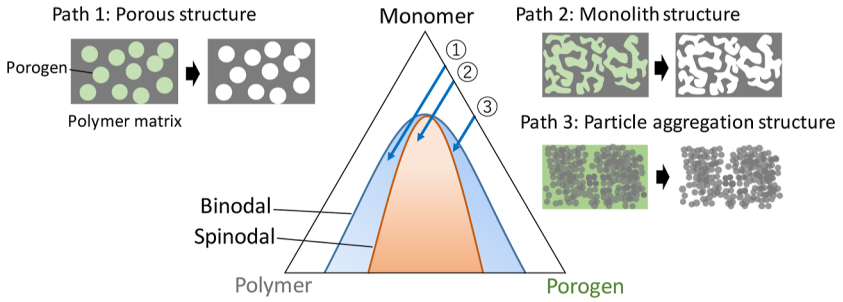

Figure 6. Model phase diagram of three components, including monomer, polymer, and progen. The amount of porogen is predetermined. Therefore, as the reaction proceeds, the ratio of monomer and polymer changes. Assuming a phase diagram shown here, the porous structure, monolith structure, and particle aggregation structure can be explained by the represented three paths. Schematic images of the microstructure formed by porogen (green) and polymer (gray) are presented. It is noted that the porogen is washed away eventually.

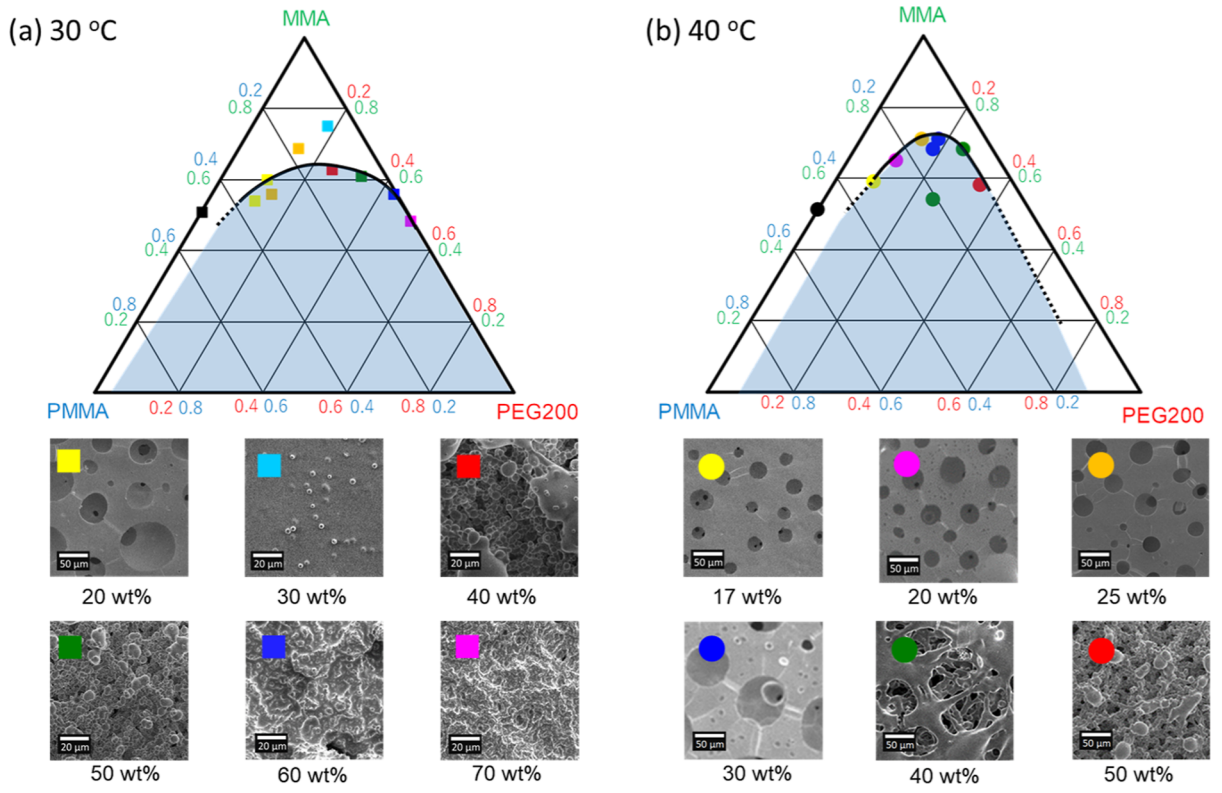

Figure 7. Apparent phase diagram during bulk polymerization of MMA in the presence of PEG (a) at 30 and (b) 40 °C, respectively. The color at the upper left of SEM images corresponds to the points with the same color in the phase diagram. Black points corresponding to the apparent phase separation are observed in the absence of PEG.

the same color. While some experimental conditions provide reproducible results, other experimental conditions lead to the deviation of the data. When 40 wt % PEG was added, the PMMA fractions at the onset of phase separation in two repeated experiments were 0.07 and 0.2. Despite the huge deviation in the onset, the final structure is not that different. These are characteristics of the nucleation process. The nucleation events are known to occur stochastically since the activation barrier needs to be overcome.[43−47] When PEG content is small, porous structures are formed. This means that the PEG particles are formed, and they are washed away. When PEG content is 40 wt % at 40 °C, co-continuous monolith structures are formed. Only a few aggregated particles are observed under this condition. This indicates that the phase separation occurred almost purely via spinodal decomposition. Above 50 wt %, aggregated particles are observed. Through nucleation and growth, aggregated PMMA particles are formed. In between 40 and 50 wt %, while the monolith structure is clearly present, the aggregated PMMA particles cover the surface. The phase separation initially occurred via the nucleation growth mechanism and subsequently via spinodal decomposition. Although there were similar approaches,[48−50] the obtained structure is limited. Co-polymerization in the mixture of MMA/vinyl acetate/poly[ethylene-*co*-(vinyl acetate)] leads only to a particle aggregation structure, at least in the investigated conditions.[49] This means PEG with a molar mass of 200 g/mol shows an excellent property as a porogen for the MMA/PMMA system. It seems that the non-reactive nature of PEG with MMA, as well as the small molar mass of PEG, is the key to the variety of phase-separated structures. In fact, our screening experiments showed that the addition of PEG with a higher molar mass (e.g., M_w = 600 g/

https://doi.org/10.1021/acsomega.2c04690
ACS Omega 2022, 7, 38933−38941

mol) in MMA generates only particle aggregation structures. We also point out that not only thermodynamic factors but also kinetic factors influence the structure. As we discussed in our previous study,[38] the apparent phase separation between MMA and PMMA cannot be accounted for based on the classical Flory−Huggins parameter in this temperature range. The dynamic heterogeneity may have played a role.[51] The molar mass distribution of the obtained PMMA is summarized in Figure S5 and in Table S1. Bimodal distribution is depicted in agreement with previous studies.[36−38] Interestingly, the amount of PEG significantly affects the molar mass distribution. When the PEG content is low, the distribution is relatively low molecular-weight rich. On the other hand, as the PEG fraction increases, the distribution becomes relatively high molecular-weight rich.

There are several potential applications for such microstructured PMMA. For demonstration purposes, we investigated surface modification using aggregated PMMA particles. It is well known that the microscopic roughness on the surface enhances wettability. In order to achieve hydrophobicity, we coated the surface of PMMA using chemical vapor deposition (CVD) as described in the literature.[8] This method fluorinates the surface with a thin chemical layer even when the surface topology is complicated. Figure 8a,b displays the SEM images

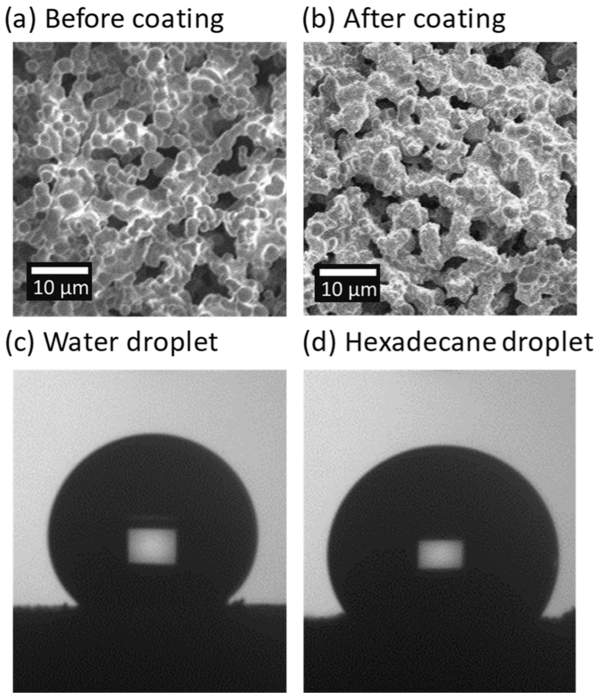

Figure 8. SEM images before (a) and after (b) the coating. The structures are kept. Contact angle measurement on the surface after the coating of the water droplet (c) and the hexadecane droplet (d). The liquid amount of water was 2 μL, and that of hexadecane was 5 μL.

before and after the coating, respectively. There are no significant differences in morphology. In Figure 8c, a sessile drop image is provided. The highest contact angle observed is 131.8°. The average advancing contact angle and receding contact angle were 132.5 and 122.1°, respectively. This surface shows not only hydrophobicity but also oleophobicity, as shown in Figure 8d. The contact angle of hexadecane is 123.0° on the same surface in Figure 8c. In other words, this surface is amphiphobic. In order to possess amphiphobicity, an overhang structure is required.[52−55] The particle aggregation structure has this characteristic. The hydrophobicity was observed only when the surface structure was a particle aggregation structure. The static contact angles of bulk and microstructured PMMA are summarized in Table 2. Using the method, amphiphobic

Table 2. Contact Angle of Water on the Structured PMMA[a]

	PEG 200 (wt %)	contact angle (°) before CVD	contact angle (°) after CVD
bulk PMMA		60.3	88.6
porous	30	58.6	18.8
co-continuous monolith	40	complete wetting	55.7[b]
particle aggregation	50	complete wetting	131.8[c]

[a]These values are obtained from the average of 10 measurements. [b]Water droplet was slowly absorbed into the structured PMMA. [c]The contact angle has a deviation depending on the position of the surface. A representative value is shown.

surfaces in a large area can be prepared relatively easily. The contact angle on the fabricated surface varies depending on the position of the surface. This is because of the different sizes of the aggregation particles. The smallest PMMA droplets we fabricated in this study are in the order of hundreds of nanometers. The fabrication of smaller particles homogeneously would be the key to improving amphiphobicity.

CONCLUSIONS

Polymerization-induced phase separation occurs during bulk polymerization of MMA in the presence of PEG. In general, phase separation is coupled with the temperature increase associated with the Trommsdorff effect. Therefore, despite the fact that PEG is a non-reactive component, the addition of PEG significantly shortens the time for reaction completion. Phase separation generates either a porous structure, a co-continuous monolith structure, or a particle aggregation structure, depending on the initial composition. The porous structure and the co-continuous monolith structure have pores whose diameter ranges from 1 to 50 μm. The particle aggregation structure has typical particle sizes of 1 to 20 μm. These structures and sizes of pores or particles can be tuned by the initial conditions. It was demonstrated that the fluorinated particle aggregation structure has an amphiphobicity with a water contact angle of 135° and a hexadecane contact angle of 105°. This simple technique can be used to fabricate microstructures in large areas cost-effectively.

ASSOCIATED CONTENT

Supporting Information

The Supporting Information is available free of charge at https://pubs.acs.org/doi/10.1021/acsomega.2c04690.

^{1}H NMR spectrum during bulk polymerization of MMA in the presence of PEG; photograph of the structured PMMA; comparison of the top view and cross-sectional view of the structured PMMA taken by SEM; photograph of UV cell after the polymerization of MMA in the presence of PEG; molar mass distribution of PMMA polymerized in the presence of different amounts of PEG; and a summary of the number-average molecular weight, weight-average molecular weight, and molecular weight distributions of PMMA formed after the

https://doi.org/10.1021/acsomega.2c04690
ACS Omega 2022, 7, 38933−38941

polymerization of MMA in the presence of PEG with different amounts (PDF)

AUTHOR INFORMATION

Corresponding Author

Yasuhito Suzuki − *Department of Applied Chemistry, Graduate School of Engineering, Osaka Prefecture University, Sakai, Osaka 599-8531, Japan; Department of Applied Chemistry, Graduate School of Engineering, Osaka Metropolitan University, Sakai, Osaka 599-8531, Japan;* orcid.org/0000-0002-5177-4079; Email: suzuki_y@omu.ac.jp

Authors

Shodai Onozato − *Department of Applied Chemistry, Graduate School of Engineering, Osaka Metropolitan University, Sakai, Osaka 599-8531, Japan*

Yuya Shinagawa − *Department of Applied Chemistry, Graduate School of Engineering, Osaka Prefecture University, Sakai, Osaka 599-8531, Japan*

Akikazu Matsumoto − *Department of Applied Chemistry, Graduate School of Engineering, Osaka Prefecture University, Sakai, Osaka 599-8531, Japan; Department of Applied Chemistry, Graduate School of Engineering, Osaka Metropolitan University, Sakai, Osaka 599-8531, Japan*

Complete contact information is available at: https://pubs.acs.org/10.1021/acsomega.2c04690

Notes

The authors declare no competing financial interest.

ACKNOWLEDGMENTS

Y.S. acknowledges the financial support by JSPS KAKENHI grant no 22K14015 and the 2022 Osaka Metropolitan University (OMU) Strategic Research Promotion Project (Young Researcher).

REFERENCES

(1) Xia, Y.; Whitesides, G. M. Soft Lithography. *Angew. Chem., Int. Ed.* **1998**, *37*, 550−575.

(2) Rose, M. A.; Bowen, J. J.; Morin, S. A. Emergent Soft Lithographic Tools for the Fabrication of Functional Polymeric Microstructures. *ChemPhysChem* **2019**, *20*, 909−925.

(3) Bacakova, L.; Filova, E.; Parizek, M.; Ruml, T.; Svorcik, V. Modulation of Cell Adhesion, Proliferation and Differentiation on Materials Designed for Body Implants. *Biotechnol. Adv.* **2011**, *29*, 739−767.

(4) Meille, V. Review on Methods to Deposit Catalysts on Structured Surfaces. *Appl. Catal., A* **2006**, *315*, 1−17.

(5) Rodriguez, A. W.; Capasso, F.; Johnson, S. G. The Casimir Effect in Microstructured Geometries. *Nat. Photonics* **2011**, *5*, 211−221.

(6) Wong, T. S.; Kang, S. H.; Tang, S. K. Y.; Smythe, E. J.; Hatton, B. D.; Grinthal, A.; Aizenberg, J. Bioinspired Self-Repairing Slippery Surfaces with Pressure-Stable Omniphobicity. *Nature* **2011**, *477*, 443−447.

(7) Mishchenko, L.; Hatton, B.; Bahadur, V.; Taylor, J. A.; Krupenkin, T.; Aizenberg, J. Design of Ice-Free Nanostructured Surfaces Based on Repulsion of Impacting Water Droplets. *ACS Nano* **2010**, *4*, 7699−7707.

(8) Deng, X.; Mammen, L.; Butt, H. J.; Vollmer, D. Candle Soot as a Template for a Transparent Robust Superamphiphobic Coating. *Science* **2012**, *335*, 67−70.

(9) Loccufier, E.; Geltmeyer, J.; Daelemans, L.; D'hooge, D. R.; De Buysser, K. D.; De Clerck, K. D. Silica Nanofibrous Membranes for the Separation of Heterogeneous Azeotropes. *Adv. Funct. Mater.* **2018**, *28*, 1804138.

(10) Hamley, I. W. Nanotechnologie Mit Weichen Materialien. *Angew. Chem.* **2003**, *115*, 1730−1752.

(11) Liu, T.; Burger, C.; Chu, B. Nanofabrication in Polymer Matrices. *Prog. Polym. Sci.* **2003**, *28*, 5−26.

(12) Barker, L. M.; Hollenbach, R. E. Shock-Wave Studies of PMMA, Fused Silica, and Sapphire. *J. Appl. Phys.* **1970**, *41*, 4208−4226.

(13) Semaltianos, N. G. Spin-Coated PMMA Films. *Microelectron. J.* **2007**, *38*, 754−761.

(14) Ligon-Auer, S. C.; Schwentenwein, M.; Gorsche, C.; Stampfl, J.; Liska, R. Toughening of Photo-Curable Polymer Networks: A Review. *Polym. Chem.* **2016**, *7*, 257−286.

(15) Yang, W.; Rallini, M.; Wang, D. Y.; Gao, D.; Dominici, F.; Torre, L.; Kenny, J. M.; Puglia, D. Role of Lignin Nanoparticles in UV Resistance, Thermal and Mechanical Performance of PMMA Nanocomposites Prepared by a Combined Free-Radical Graft Polymerization/Masterbatch Procedure. *Composites, Part A* **2018**, *107*, 61−69.

(16) Moens, E. K. C.; De Smit, K. D.; Marien, Y. W.; Trigilio, A. D.; Van Steenberge, P. H. M.; Van Geem, K. M. V.; Dubois, J. L.; D'hooge, D. R. Progress in Reaction Mechanisms and Reactor Technologies for Thermochemical Recycling of Poly(methyl methacrylate). *Polymers* **2020**, *12*, 1667.

(17) Yoneda, S.; Han, W.; Hasegawa, U.; Uyama, H. Facile Fabrication of Poly(Methyl Methacrylate) Monolith via Thermally Induced Phase Separation by Utilizing Unique Cosolvency. *Polymer* **2014**, *55*, 3212−3216.

(18) Kimura, N.; Kawazoe, K.; Nakanishi, H.; Norisuye, T.; Tran-Cong-Miyata, Q. Influences of Wetting and Shrinkage on the Phase Separation Process of Polymer Mixtures Induced by Photopolymerization. *Soft Matter* **2013**, *9*, 8428−8437.

(19) Sicher, A.; Ganz, R.; Menzel, A.; Messmer, D.; Panzarasa, G.; Feofilova, M.; Prum, R. O.; Style, R. W.; Saranathan, V.; Rossi, R. M.; Dufresne, E. R. Structural Color from Solid-State Polymerization-Induced Phase Separation. *Soft Matter* **2021**, *17*, 5772−5779.

(20) Tsujioka, N.; Hira, N.; Aoki, S.; Tanaka, N.; Hosoya, K. A New Preparation Method for Well-Controlled 3D Skeletal Epoxy Resin-Based Polymer Monoliths Norio. *Macromolecules* **2005**, *38*, 9901−9903.

(21) Tsujioka, N.; Ishizuka, N.; Tanaka, N.; Kubo, T.; Hosoya, K. Well-Controlled 3D Skeletal Epoxy-Based Monoliths Obtained by Polymerization Induced Phase Separation. *J. Polym. Sci., Part A: Polym. Chem.* **2008**, *46*, 3272−3281.

(22) Buchmeiser, M. R. Polymeric Monolithic Materials: Syntheses, Properties, Functionalization and Applications. *Polymer* **2007**, *48*, 2187−2198.

(23) Wu, R.; Hu, L.; Wang, F.; Ye, M.; Zou, H. Recent Development of Monolithic Stationary Phases with Emphasis on Microscale Chromatographic Separation. *J. Chromatogr. A* **2008**, *1184*, 369−392.

(24) Uehara, F.; Matsumoto, A. Metal-resin Bonding Mediated by Epoxy Monolith Layer. *Appl. Adhes. Sci.* **2016**, *4*, 18.

(25) Sugimoto, Y.; Nishimura, Y.; Uehara, F.; Matsumoto, A. Dissimilar Materials Bonding Using Epoxy Monolith. *ACS Omega* **2018**, *3*, 7532−7541.

(26) Sakata, N.; Takeda, Y.; Kotera, M.; Suzuki, Y.; Matsumoto, A. Interfacial Structure Control and Three-Dimensional X-Ray Imaging of an Epoxy Monolith Bonding System with Surface Modification. *Langmuir* **2020**, *36*, 10923−10932.

(27) Tominaga, R.; Nishimura, Y.; Suzuki, Y.; Takeda, Y.; Kotera, M.; Matsumoto, A. Co-Continuous Network Polymers Using Epoxy Monolith for the Design of Tough Materials. *Sci. Rep.* **2021**, *11*, 1431.

(28) Flory, P. J. *Principles of Polymer Chemistry*; Cornell University Press, 1953.

(29) Tulig, T. J.; Tirrell, M. On the Onset of the Trommsdorff Effect. *Macromolecules* **1982**, *15*, 459−463.

(30) Achilias, D. S. A Review of Modeling of Diffusion Controlled Polymerization Reactions. *Macromol. Theory Simul.* **2007**, *16*, 319−347.
(31) Johnston-Hall, G.; Monteriro, M. J. Bimolecular Radical Termination: New Perspectives and Insights. *J. Polym. Sci., Part A: Polym. Chem.* **2008**, *46*, 3155−3173.
(32) Trigilio, A. D.; Marien, Y. W.; Van Steenberge, P. H. M.; D'hooge, D. R. Gillespie-Driven kinetic Monte Carlo Algorithms to Model Events for Bulk or Solution (Bio)Chemical Systems Containing Elemental and Distributed Species. *Ind. Eng. Chem. Res.* **2020**, *59*, 18357−18386.
(33) De Smit, K.; Marien, Y. W.; Van Geem, K. M.; Van Steenberge, P. H. M.; D'hooge, D. R. Connecting polymer synthesis and chemical recycling on a chain-by-chain basis: a unified matrix-based kinetic Monte Carlo strategy. *React. Chem. Eng.* **2020**, *5*, 1909−1928.
(34) Stempfle, B.; Dill, M.; Winterhalder, M. J.; Müllen, K.; Wöll, D. Single Molecule Diffusion and Its Heterogeneity during the Bulk Radical Polymerization of Styrene and Methyl Methacrylate. *Polym. Chem.* **2012**, *3*, 2456−2463.
(35) Nölle, J. M.; Primpke, S.; Müllen, K.; Vana, P.; Wöll, D. Diffusion of Single Molecular and Macromolecular Probes during the Free Radical Bulk Polymerization of MMA-towards a Better Understanding of the Trommsdorff Effect on a Molecular Level. *Polym. Chem.* **2016**, *7*, 4100−4105.
(36) Suzuki, Y.; Shinagawa, Y.; Kato, E.; Mishima, R.; Fukao, K.; Matsumoto, A. Polymerization-Induced Vitrification and Kinetic Heterogenization at the Onset of the Trommsdorff Effect. *Macromolecules* **2021**, *54*, 3293−3303.
(37) Tran-Cong-Miyata, Q.; Nakanishi, H. Phase separation of polymer mixtures driven by photochemical reactions: current status and perspectives. *Polym. Int.* **2017**, *66*, 213−222.
(38) Suzuki, Y.; Cousins, D. S.; Shinagawa, Y.; Bell, R. T.; Matsumoto, A.; Stebner, A. P. Phase Separation during Bulk Polymerization of Methyl Methacrylate. *Polym. J.* **2019**, *51*, 423−431.
(39) West, A. G.; Barner-Kowollik, C.; Perrier, S. Poly(ethylene glycol) as a 'green solvent' for the RAFT polymerization of methyl methacrylate. *Polymer* **2010**, *51*, 3836−3842.
(40) Suzuki, Y.; Mishima, R.; Matsumoto, A. Bulk Polymerization Kinetics of Methyl Methacrylate at Broad Temperature Range Investigated by Differential Scanning Calorimetry. *Int. J. Chem. Kinet.* **2022**, *54*, 361−370.
(41) Suzuki, Y.; Cousins, D.; Wassgren, J.; Kappes, B. B.; Dorgan, J.; Stebner, A. P. Kinetics and Temperature Evolution during the Bulk Polymerization of Methyl Methacrylate for Vacuum-Assisted Resin Transfer Molding. *Composites, Part A* **2018**, *104*, 60−67.
(42) Inoue, T. Reaction-Induced Phase Decomposition in Polymer Blends. *Prog. Polym. Sci.* **1995**, *20*, 119−153.
(43) Flory, P. J. Thermodynamics of high polymer solutions. *J. Chem. Phys.* **1941**, *9*, 660.
(44) Huggins, M. L. Solution of long-chain compounds. *J. Chem. Phys.* **1941**, *9*, 440.
(45) Kondepudi, D. K.; Asakura, K. Chiral Autocatalysis, Spontaneous Symmetry Breaking, and Stochastic Behavior. *Acc. Chem. Res.* **2001**, *34*, 946−954.
(46) Rao, F.; Ding, K.; Zhou, Y.; Zheng, Y.; Xia, M.; Lv, S.; Song, Z.; Feng, S.; Ronneberger, I.; Mazzarello, R.; Zhang, W.; Ma, E. Reducing the stochasticity of crystal nucleation to enable subnanosecond memory writing. *Science* **2017**, *358*, 1423−1427.
(47) Suzuki, Y.; Steinhart, M.; Butt, H.-J.; Floudas, G. Kinetics of Ice Nucleation Confined in Nanoporous Alumina. *J. Phys. Chem. B* **2015**, *119*, 11960−11966.
(48) Chen, W.; Kobayashi, S.; Inoue, T.; Ohnaga, T.; Ougizawa, T. Polymerization-Induced Spinodal Decomposition of Poly(Ethylene-Co-Vinyl Acetate) Methyl Methacrylate Mixture and the Influence of Incorporating Poly(Vinyl Acetate) Macromonomer. *Polymer* **1994**, *35*, 4015−4021.
(49) Chen, W.; Li, X.; Jiang, M. Spinodal Decomposition Induced by Copolymerization in the Mixture of Methyl Methacrylate/Vinyl Acetate/Poly[Ethylene-Co-(Vinyl Acetate)]. *Macromol. Chem. Phys.* **1998**, *199*, 319−325.
(50) Cheng, S. K.; Wang, C. C.; Chen, C. Y. Study on the Phase Behavior of EVA/PS Blends During in Situ Polymerization. *Polym. Eng. Sci.* **2003**, *43*, 1221−1231.
(51) Tanaka, H. Viscoelastic Phase Separation. *J. Phys. Condens. Matter* **2000**, *12*, R207.
(52) Shibuichi, S.; Yamamoto, T.; Onda, T.; Tsujii, K. Super Water- and Oil-Repellent Surfaces Resulting from Fractal Structure. *J. Colloid Interface Sci.* **1998**, *208*, 287.
(53) Chen, W.; Fadeev, A. Y.; Hsieh, M. C.; Öner, D.; Youngblood, J.; McCarthy, T. J. Ultrahydrophobic and Ultralyophobic Surfaces: Some Comments and Examples. *Langmuir* **1999**, *15*, 3395.
(54) Steele, A.; Bayer, I.; Loth, E. Inherently Superoleophobic Nanocomposite Coatings by Spray Atomization. *Nano Lett.* **2009**, *9*, 501.
(55) Tuteja, A.; Choi, W.; Ma, M. L.; Mabry, M. L.; Mazzella, J. M.; Rutledge, S. A.; McKinley, G. H.; Cohen, R. E. Designing Superoleophobic Surfaces. *Science* **2007**, *318*, 1618.

https://doi.org/10.1021/acsomega.2c04690
ACS Omega 2022, 7, 38933−38941